

# Slicing the Swaption Cube

Thomas Mazzoni

University of Greifswald, Germany, e-mail: thomas.mazzoni@uni-greifswald.de

## Abstract

In this paper, a new parametric model for the implied volatility surface of swaptions is introduced. It is based on the theoretical representation of local variance as the bridge expectation of actual variance at expiry, and uses a specially tailored GARCH model to compute this expectation. The resulting model is calibrated to an extended swaption cube data example and extracts a discrete set of volatility surfaces, organized by the tenor of the underlying swap contract. The subsequent analysis indicates that the model fit is very precise and the approach is superior to currently available competing parametric models. Finally, it is shown that the new method generates more realistic dynamics than non-parametric models, which qualifies it for hedging and risk management purposes.

## Keywords

swaption cube, volatility surface, bridge process, GARCH models, most likely path approximation

JEL codes: C58, G13

## 1 Introduction

Nowadays, large parts of modern derivative pricing rely on the implied volatility surface. That is because the Black–Scholes formula (Black and Scholes, 1973; Merton, 1973) is widely used as a metric to quote option prices in terms of their strike, time to expiry, and implied volatility. In the same tradition, large parts of the fixed-income market are built around the Black-76 model (Black, 1976). Originally, the purpose of this model was the pricing of options on futures and forward contracts. But since different numéraires give rise to different equivalent martingale measures, Black's formula is used for pricing of bond options, interest rate caps and floors, and swaptions too. In all cases, knowledge of the implied volatility surface grants immediate access to the fair market price of the respective derivative for all combinations of strike and expiry. Furthermore, a parametric surface model permits analytic computation of the Greeks, which is most important in hedging and risk management.

Even though ordinary stock and index options are priced inside the same model framework as options on interest and swap rates, there are significant differences in the observed behavior of both types of underlying. The return processes in equity markets were known to exhibit heteroscedasticity, volatility clustering, and leptokurtosis for a very long time. This fact was, on the one hand, reflected in econometrics by the development of GARCH models (Engle, 1982; Bollerslev, 1986) and the respective option pricing theory due to Duan (1995), Heston and Nandi (1997, 2000), and others. On the other hand, refinements of the Black–Scholes

theory were suggested. An incomplete list of pioneering improvements is Merton (1976), Heston (1993), Bates (1996), and Hagan *et al.* (2002). Fixed-income models started with the short-rate models of Vasicek (1977), Dothan (1978), and Cox *et al.* (1985), and evolved over multifactor models to the seminal HJM framework of Heath *et al.* (1992). More recent successors are the LIBOR and swap-market models of Brace *et al.* (1997) and Jamshidian (1997). Before the mid-1990s, forward-rate smiles were monotonically decaying and were not even observed in currencies other than the JPY (cf. Rebonato *et al.*, 2009, p. 150, fn. 3). The stylized facts of equity return volatility are still not that emphasized in fixed-income markets, but clearly distinct enough to be considered in recent models.

There is another important feature in fixed-income markets that is absent in the equity market: the term structure of the at-the-money (ATM) volatility, hereafter called the backbone of the volatility surface. Volatilities of forward rates with both short and long time to maturity are rather moderate, whereas for mid-term maturities, volatility usually exhibits a humped shape with a maximum at about 2 to 3 years. Rebonato (2004, p. 672) attributes this behavior to the monetary policy of central bank authorities. In the short run, they tend to keep their actions predictable, whereas in the long run, movements are smoothly adjusted due to inflation targeting. This characteristic shape of the ATM volatility depends nearly exclusively on the time to maturity of the respective rate, which qualifies it as a stylized fact.

A parametrization of the implied volatility surface has to accommodate these stylized features in order to be applicable in equity and fixed-income scenarios. A framework suitable for equity markets, based on a GARCH vehicle, was introduced in Mazzoni (2015). To derive a model framework that extends to the swaption market and generates sufficiently precise implied volatility surfaces, this approach is generalized in two ways. Firstly, the natural model period of one trading day is replaced by an arbitrary time interval. In equity markets, time series models based on daily open or closing prices of assets are quite successful, but a swap rate, for example, can be understood as a dynamically weighted average of certain forward rates. The natural timing for those rates may differ considerably. Secondly, the initial GARCH variance is equipped with a dependency on time to maturity, to accommodate the term structure of the ATM volatility.

The rest of the paper is organized as follows. Section 2 provides the theoretical background and derives the parametric model for the implied volatility. This model is calibrated to an extended volatility cube data example in Section 3. The results for the original model and some reduced versions of it are analyzed too. In Section 4, the suggested approach is benchmarked against other parametric models for the implied volatility surface, as far as they are available. Section 5 investigates the dynamic behavior of the parametric model with respect to a generic non-parametric implied volatility surface. Finally, Section 6 summarizes the findings and draws some conclusions.



## TECHNICAL PAPER

## 2 Theoretical framework

### 2.1 Black's formula

The common metric for the price of a European call option at time  $t$ , with strike  $K$  and expiry  $T$ , is Black's formula

$$C_t^B(K, T) = \mathcal{N}(t)(F_t \Phi(d_+) - K \Phi(d_-)), \quad (1)$$

with

$$d_{+-} = \frac{\log(F_t/K) \pm \frac{1}{2}\sigma_{\text{imp}}^2(T-t)}{\sigma_{\text{imp}}\sqrt{T-t}}. \quad (2)$$

In Eq. (1),  $\mathcal{N}(t)$  is the numéraire associated with the equivalent martingale measure that makes the process  $F_t$  driftless. For a non-dividend-paying stock, the numéraire is the discount bond  $P(t, T)$ , the associated measure is the  $T$ -forward measure  $Q_T$ , and  $F_t$  is the forward price of the stock  $S$  at time  $t$ ,

$$Q_T : \quad \mathcal{N}(t) = P(t, T) \text{ and } F_t = S_t/P(t, T). \quad (3)$$

Under the annuity measure  $A_{T,N}$ , Black's formula yields the price of a payer swap with expiry  $T = T_0$  on the forward swap rate  $F_t = r_N(t, T)$ ,

$$A_{T,N} : \quad \mathcal{N}(t) = \sum_{n=1}^N (T_n - T_{n-1})P(t, T_n) \text{ and } F_t = r_N(t, T). \quad (4)$$

In both cases, knowledge of  $F_t$  and  $\sigma_{\text{imp}}(K, T)$  is sufficient to extract option prices for arbitrary strikes  $K$  and expiries  $T$ .

### 2.2 The relation of actual, local, and implied volatility

For the remainder of the paper, assume without loss of generality that today is time  $t = 0$ . Consider the geometric model

$$dF_t = \mu(t)F_t dt + \sigma(F_t, t)F_t dW_t \quad (5)$$

for the price process of an arbitrary underlying  $F$ , where  $W_t$  is a standard Brownian motion and actual volatility  $\sigma(F_t, t)$  may or may not be a random function itself. Based on the work of Breeden and Litzenberger (1978), Dupire (1994) concluded that there has to be a smooth deterministic function  $\sigma_{\text{loc}}(F, t)$ , the local volatility, such that the process

$$dF_t = \mu(t)F_t dt + \sigma_{\text{loc}}(F_t, t)F_t dW_t \quad (6)$$

generates the prices of all European call options on the underlying  $F$ , observed in the market. Further research due to Dupire (1996, 2004) and Derman and Kani (1998) revealed the connection between actual and local volatility,

$$\sigma_{\text{loc}}^2(K, T) = E^Q[\sigma^2(F_T, T)|F_T = K]. \quad (7)$$

That is, local variance  $\sigma_{\text{loc}}^2(K, T)$  is the expectation of actual variance  $\sigma^2(F_T, T)$  under the pricing measure  $Q$ , conditional on  $F_T = K$ , as seen from today,  $t = 0$ . Implied variance can be recovered approximately as the average local variance along the most likely path  $\hat{F}_t$  from  $F_0$  at  $t = 0$  to  $K$  at  $t = T$ ,

$$\sigma_{\text{imp}}^2(K, T) \approx \frac{1}{T} \int_0^T \sigma_{\text{loc}}^2(\hat{F}_t, t) dt. \quad (8)$$

This idea is due to Gatheral (2006, chap. 3) and was made completely rigorous by Keller-Ressel and Teichmann (2009). Usually, the most likely path itself can be approximated sufficiently accurately by a straight line in log-price space.

The suggested method uses a particularly modified discrete-time GARCH model to compute local volatility in terms of the conditional expectation (7), and afterwards the most likely path formalism (8) is applied to extract an analytic representation of the implied volatility surface.

### 2.3 Discrete-time Gaussian bridge process

Let  $F_t$  be a  $Q$ -martingale and  $x_t = \log F_t$  for  $0 \leq t \leq T$ , where  $T$  is the expiry of the European-style contingent claim on  $F$  under consideration. The discrete process

$$x_t = x_{t-\Delta t} - \frac{1}{2}h_t(T)\Delta t + \varepsilon_t \quad (9)$$

with  $\varepsilon_t = \sqrt{h_t(T)\Delta t} \cdot z_t$  and  $z_t \sim N(0, 1)$  makes the underlying a  $Q$ -martingale,  $F_t = E^Q[F_{t+n\Delta t}|F_t]$  for  $n = 1, \dots, N$ , if the process  $h_{t+\Delta t}(T)$  is  $F_t$ -predictable. To see this, note that

$$E^Q[F_{t+\Delta t}|F_t] = E^Q\left[F_t e^{-\frac{1}{2}h_{t+\Delta t}(T)\Delta t + \varepsilon_{t+\Delta t}}|F_t\right] = F_t, \quad (10)$$

and use iterated expectations. Subsequently,  $h_t(T)$  will be given GARCH dynamics, but it is not necessary to specify a particular model at this point.

To make sure that the process  $x_t$  crosses the logarithmic strike  $k = \log K$  at time  $t = T$ , the increment  $z_t$  is replaced by a conditional Gaussian bridge increment  $\zeta_t$ , with moments

$$E^Q[\zeta_t|F_{t-\Delta t}] = \sqrt{\frac{\Delta t}{h_t(T)}} \cdot \frac{k - x_{t-\Delta t}}{T - t + \Delta t} + \frac{1}{2}\sqrt{h_t(T)\Delta t} \quad (11)$$

and

$$\text{Var}[\zeta_t] = 1 - \frac{\Delta t}{T - t + \Delta t}. \quad (12)$$

The "unconditional" expectation of  $x_t$  with respect to this bridge increment is

$$E^Q[x_t|F_{0 \rightarrow k}] = \frac{t}{T}k + \left(1 - \frac{t}{T}\right)x_0, \quad (13)$$

where the slightly abusive notation  $F_{0 \rightarrow k}$  was used as shorthand for the information  $F_0 \cap \{x_T = k\}$ . The proof of Eq. (13) is provided in Appendix A. Obviously, for  $t = T$  one obtains  $E^Q[x_T|F_{0 \rightarrow k}] = k$ , as desired. To show that  $x_t$  is indeed a bridge process, one can use the variance decomposition to compute

$$\begin{aligned} \text{Var}^Q[x_T|F_{0 \rightarrow k}] &= \text{Var}^Q[E^Q[x_T|F_{T-\Delta t \rightarrow k}]|F_{0 \rightarrow k}] \\ &\quad + E^Q[\text{Var}^Q[x_T|F_{T-\Delta t \rightarrow k}]|F_{0 \rightarrow k}] \\ &= \text{Var}^Q[k|F_{0 \rightarrow k}] + E^Q[h_T(T)\Delta t \cdot 0|F_{0 \rightarrow k}] = 0. \end{aligned} \quad (14)$$

Thus, the process  $x_t$ , when supplied with the bridge increment  $\zeta_t$ , is indeed a bridge process from  $x_0 = \log F_0$  to  $x_T = \log K$ . Furthermore, the expected path is the straight line (13), and all increments are conditionally Gaussian. Thus, the process  $x_t$  can be regarded as a conditional version of a Brownian bridge, and local variance is given by the expectation

$$\sigma_{\text{loc}}^2(K, T) = E^Q[h_T(T)|F_{0 \rightarrow k}]. \quad (15)$$

It is usually very difficult to compute this expectation, because one has to exploit a recursive pattern with respect to a conditional random error. But there is a particular class of GARCH models, permitting an explicit approximation, introduced next.

## 2.4 GARCH volatility dynamics

As detailed in Mazzoni (2015), the class of asymmetric GARCH (AGARCH) models introduced by Engle (1990),

$$h_t(T)\Delta t = \omega + \sum_{p=1}^P \alpha_p (\varepsilon_{t-p\Delta t} - \gamma_p)^2 + \sum_{q=1}^Q \beta_q h_{t-q\Delta t}(T) \Delta t, \quad (16)$$

permits an approximate recursive computation of the conditional variance. It was also shown that the AGARCH(1,1) already accommodates the typical short-term smile and long-term skew of an implied volatility surface. Higher model orders were analyzed in Mazzoni (2015), but did not show considerable improvements. Therefore, the (1,1)-representative of the AGARCH family is used in the sequel. After dividing by  $\Delta t$ , one obtains

$$h_t(T) = \frac{\omega}{\Delta t} + \frac{\alpha}{\Delta t} (\varepsilon_{t-\Delta t} - \gamma)^2 + \beta h_{t-\Delta t}(T). \quad (17)$$

The aim of this section is to derive an explicit approximation for  $E^Q[h_T(T)|\mathcal{F}_{0 \rightarrow k}]$ . To this end, it is necessary to compute the unconditional bridge expectation of the random error  $\varepsilon_t$ . The conditional expectation due to Eq. (11) is

$$E^Q[\varepsilon_t|\mathcal{F}_{t-\Delta t \rightarrow k}] = \Delta t \left( \frac{k - x_{t-\Delta t}}{T - t + \Delta t} + \frac{1}{2} h_t(T) \right). \quad (18)$$

Applying the expectation operator  $E^Q[\dots|\mathcal{F}_{0 \rightarrow k}]$  on both sides of Eq. (18) yields the desired quantity

$$E^Q[\varepsilon_t|\mathcal{F}_{0 \rightarrow k}] = \Delta t \left( \frac{k - x_0}{T} + \frac{1}{2} E^Q[h_t(T)|\mathcal{F}_{0 \rightarrow k}] \right). \quad (19)$$

To declutter the notation, the reference to the probability measure and the information set is omitted for the rest of this section, which means that  $E[\dots] = E^Q[\dots|\mathcal{F}_{0 \rightarrow k}]$ . Taking expectations on both sides of Eq. (17) yields

$$\begin{aligned} E[h_t(T)] &= \frac{\omega}{\Delta t} + \frac{\alpha}{\Delta t} E[(\varepsilon_{t-\Delta t} - \gamma)^2] + \beta E[h_{t-\Delta t}(T)] \\ &= \frac{\omega}{\Delta t} + \frac{\alpha}{\Delta t} \text{Var}[\varepsilon_{t-\Delta t}] + \frac{\alpha}{\Delta t} (E[\varepsilon_{t-\Delta t}] - \gamma)^2 + \beta E[h_{t-\Delta t}(T)], \end{aligned} \quad (20)$$

where the relation  $\text{Var}[\varepsilon_t] = E[\varepsilon_t^2] - E[\varepsilon_t]^2$  was used in the second row. To compute the variance term in Eq. (20), again use the variance decomposition to obtain

$$\begin{aligned} \text{Var}[\varepsilon_t] &= E[\text{Var}[\varepsilon_t|\mathcal{F}_{t-\Delta t \rightarrow k}]] + \text{Var}[E[\varepsilon_t|\mathcal{F}_{t-\Delta t \rightarrow k}]] \\ &= E[h_t(T)\Delta t \cdot \frac{T-t}{T-t+\Delta t} + \Delta t^2 \text{Var}\left(\frac{k-x_{t-\Delta t}}{T-t+\Delta t} + \frac{1}{2} h_t(T)\right)]. \end{aligned} \quad (21)$$

The second term in the last row is negligible compared to the first one, because the variance of the conditional expectation is naturally much smaller than the variance of  $\varepsilon_t$  itself for most  $t < T$ . For the same  $t$  values, the final factor in the first term is approximately equal to one. Thus, for most  $t < T$ , the variance of the bridged random error is approximately

$$\text{Var}[\varepsilon_t] \approx E[h_t(T)]\Delta t, \quad (22)$$

which is the variance of the unbridged random error. That makes Eq. (20) into

$$E[h_t(T)] = \frac{\omega}{\Delta t} + \frac{\alpha}{\Delta t} \left( \eta + \frac{\Delta t}{2} E[h_{t-\Delta t}(T)] \right)^2 + (\alpha + \beta) E[h_{t-\Delta t}(T)], \quad (23)$$

with  $\eta = \frac{k-x_0}{T/\Delta t} - \gamma$ . Expanding the square bracket generates one term of order  $E[\dots]^2$ . Without this term, Eq. (23) would be a simple linear recursion formula. In the original paper (Mazzoni, 2015),  $E[h_t(T)]$  was computed in terms of a perturbation series, where the unperturbed solution was the one neglecting the square expectation. A subsequent analysis revealed that the relative error of the unperturbed solution was already smaller than 1 percent. Thus, simply neglecting the quadratic term yields the recursion

$$E[h_t(T)] = \frac{A}{\Delta t} + BE[h_{t-\Delta t}(T)], \quad (24)$$

with

$$A = \omega + \alpha\eta^2, \quad B = \alpha(1 + \eta) + \beta, \quad \text{and } \eta = \frac{k - x_0}{T/\Delta t} - \gamma. \quad (25)$$

For  $N = \frac{T}{\Delta t}$ , this recursion is easily computed to obtain the desired expectation value with respect to the bridge increment,

$$E[h_T(T)] = \frac{A}{\Delta t} \sum_{n=0}^{N-1} B^n + B^N h_0(T) = \frac{A}{\Delta t} \cdot \frac{1 - B^{T/\Delta t}}{1 - B} + B^{T/\Delta t} h_0(T), \quad (26)$$

where a standard geometric series result was used in the second step. Local volatility is the square root of Eq. (26), where the term structure of the backbone can be modeled by the function  $h_0(T)$ .

## 2.5 Parametric implied volatility surface

In stock markets, the backbone has very little term structure, albeit practitioners occasionally consider some kind of transition from short-term to stationary variance and long-term interest rate contributions (see Reghai, 2015, chap. 2, sec. B). In fixed-income markets, the situation is different. There are two dominant patterns, dependent on the current market regime, a hump-shaped term structure in “normal” market states and an exponentially decaying term structure in “excited” states, see for example Rebonato *et al.* (2009, sec. 4.8). Both patterns can be accommodated by the customary parametrization due to Nelson and Siegel (1987),

$$\sqrt{h_0(T)} = a + (b + cT)e^{-dT}. \quad (27)$$

Thus, local variance can be expressed as

$$\sigma_{\text{loc}}^2(K, T) = \frac{A}{\Delta t} \cdot \frac{1 - B^{T/\Delta t}}{1 - B} + B^{T/\Delta t} h_0(T), \quad (28)$$

with

$$\begin{aligned} A &= \omega + \alpha\eta^2, \quad B = \alpha(1 + \eta) + \beta, \quad \eta = \frac{\log(K/F_0)}{T/\Delta t} - \gamma, \\ \text{and } h_0(T) &= (a + (b + cT)e^{-dT})^2. \end{aligned} \quad (29)$$

In computing implied volatility, Gatheral’s most likely path approximation Eq. (8) is used, where the relevant path  $\hat{F}_t$  is assumed to be a straight line in log-price space. Using the fact that  $T = N\Delta t$ , one obtains

$$\begin{aligned} \sigma_{\text{imp}}^2(K, T) &= \frac{1}{N+1} \sum_{n=0}^N \sigma_{\text{loc}}^2(F_0^{1-\frac{n}{N}}, K^{\frac{n}{N}}, n\Delta t) \\ &= \frac{1}{N+1} \sum_{n=0}^N \frac{A}{\Delta t} \cdot \frac{1 - B^n}{1 - B} + B^n h_0(T), \end{aligned} \quad (30)$$

## TECHNICAL PAPER

with  $A$  and  $B$  as in Eq. (29). The second equality holds, because  $\eta$  is invariant under the simultaneous transformation  $K \rightarrow F_0^{1-\frac{n}{N}} \cdot K^{\frac{n}{N}}$  and  $T \rightarrow n\Delta t$ . This can be seen by plugging the transformation into the definition of  $\eta$ ,

$$\begin{aligned}\eta &= \frac{(1 - \frac{n}{N}) \log F_0 + \frac{n}{N} \log K - \log F_0}{n} - \gamma \\ &= \frac{\log K - \log F_0}{N} - \gamma = \frac{\log(K/F_0)}{T/\Delta t} - \gamma.\end{aligned}\quad (31)$$

It is now straightforward to compute the sum in Eq. (30). Again using the geometric series result, one obtains

$$\sigma_{\text{imp}}(K, T) = \sqrt{\frac{A/\Delta t}{1-B} + \frac{1}{T/\Delta t + 1} \left( h_0(T) - \frac{A/\Delta t}{1-B} \right) \frac{1-B^{T/\Delta t+1}}{1-B}}, \quad (32)$$

with  $A$ ,  $B$ , and  $h_0(T)$  as in Eq. (29). This is the desired explicit expression for implied volatility to be calibrated to observed market data in the next section. Note that Eq. (32) is a fully autonomous continuous surface parametrization. The only remnant of the discrete-time GARCH vehicle is the parameter  $\Delta t$ .

### 3 Calibration to real swaption data

#### 3.1 Full model calibration

To demonstrate the suggested method, the comprehensive EUR market swaption data example provided in Brigo and Mercurio (2007, pp. 512–513) is used. This particular data set was chosen on the one hand, because swaption data is usually only available through commercial services; on the other hand, the authors provide the full volatility cube, which means implied volatility data with respect to the strike rate, the expiry of the respective swaption, and the tenor of the underlying swap. Furthermore, they also provide fine-grained discount bond data, from which the forward swap rate can be stripped. The entire data is reproduced in Appendix B for reference.

In particular, one side of the swaption cube is partitioned in expiries of 5, 10, 20, and 30 years of the payer swaption, and tenors of 2, 5, 10, 20, and 30 years of the underlying swap contract. There is intermediate ATM volatility data that can be used naturally to calibrate the implied volatility surface. This is an advantage over conventional models like the SABR of Hagan *et al.* (2002), which are fitted to particular expiries and have to interpolate in between.

The numéraire asset in case of swaption valuation is a portfolio of discount bonds called the annuity,

$$A_{T,N}(t) = \sum_{n=1}^N (T_n - T_{n-1}) P(t, T_n), \quad (33)$$

which induces an equivalent martingale measure  $A_{T,N}$ , under which the forward swap rate process

$$r_N(t, T) = \frac{P(t, T_0) - P(t, T_N)}{A_{T,N}(t)} \quad (34)$$

is naturally driftless.

There is, however, a complication usually not present in equity markets, interrupting the connection to local volatility. Since the forward swap rate  $r_N(t, T)$  is a martingale only with respect to the measure  $A_{T,N}$ , one is really looking at a continuum of different forward swap rates, instead of one unique underlying. Consequently, the implied volatility surface is not attached to one particular swap rate, since for every rate there is at most one traded swaption. One consequence is

that forward swap rates are not driftless in the majority of available annuity measures. In order to apply Dupire's local volatility theory, the drift under a common pricing measure not only has to be known, but also has to be deterministic, see Eq. (6). In equity markets, it is common practice to assume a deterministic term structure, because the underlying is usually not very interest rate sensitive and in this case the  $T$ -forward and the risk-neutral measure coincide, which remedies the problem. This is, of course, no longer possible in fixed-income markets, because underlyings are highly interest rate sensitive here.<sup>1</sup>

Given the respective implied volatility, a plain vanilla European interest rate payer swaption is valued in the market by Black's formula Eq. (1). The criterion chosen here to be minimized in the calibration process is the unweighted root mean square error

$$\text{RMSE} = \sqrt{\frac{1}{M} \sum_{m=1}^M \left( \sigma_{\text{imp}}^{(m)} - \hat{\sigma}_{\text{imp}}^{(m)} \right)^2}, \quad (35)$$

where  $\hat{\sigma}_{\text{imp}}^{(m)}$  is the estimated implied volatility at strike  $K$  and expiry  $T = T_0$  of the  $m$ th data point. There is a total of  $M = 43$  data points contained in every tenor slice of the volatility cube. The resulting surfaces are shown in Figure 1. The observed volatilities are indicated by red dots, whereas the forward swap rate (i.e., the backbone) is traced out in gray. Visual inspection suggests a good fit of the parametric implied volatility surface. The respective parameter estimates and the root mean square error in basis points (bps) are provided in Table 1. The average RMSE is about 41 bps, which is indeed a very promising result for a nine-parameter fit of the entire implied volatility surface. With the calibrated parameters for the different tenors of the underlying interest rate swap, the volatility cube effectively reduces to a stack of volatility surfaces, represented by the respective parameters in Table 1.

#### 3.2 Calibration of reduced parametric models

There are basically two options to reduce the number of parameters of the suggested model. Both are related to the term structure of the backbone Eq. (27). In the limit for large  $T$ , the function  $h_0(T)$  becomes a constant,

$$\lim_{T \rightarrow \infty} h_0(T) = a^2. \quad (36)$$

But on the other hand, it is easily seen from Eqs. (29) and Eq. (32) that for  $\alpha(1-\gamma) + \beta < 1$ ,  $h_0(T)$  does not contribute to the implied volatility in the limit, because

$$\lim_{T \rightarrow \infty} \sigma_{\text{imp}}(K, T) = \sqrt{\frac{A/\Delta t}{1-B}}, \quad (37)$$

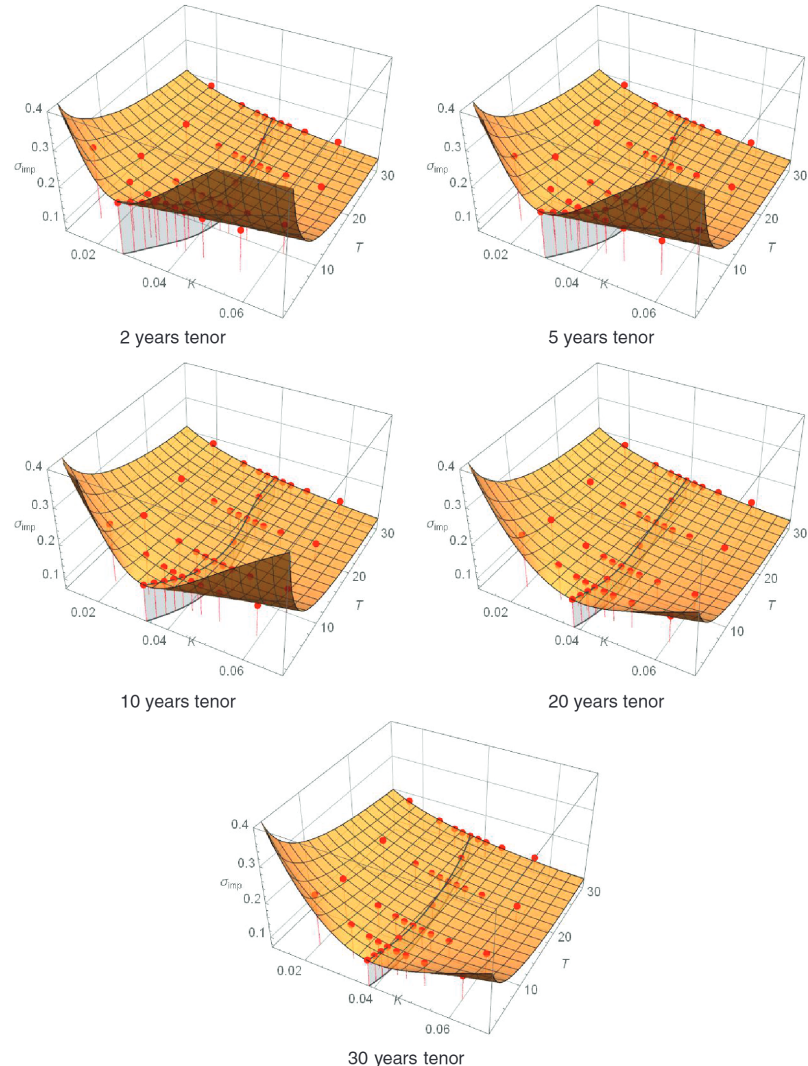
with

$$A = \omega + \alpha\gamma^2 \quad \text{and} \quad B = \alpha(1-\gamma) + \beta \quad (38)$$

holds. That means, in the limit  $T \rightarrow \infty$ , implied volatility is flat and depends only on the initial GARCH parameters. Because the long-term behavior is dominated by those quantities, one can eliminate the parameter  $a$  in Eq. (27). The results of the eight-parameter fit are provided in Table 2. The increase in RMSE is minute. Furthermore, the parameter  $c$  is estimated as very small, which means that a seven-parameter fit would most likely accommodate the observed data equally well.

The next possible level of reduction is to neglect the entire term structure of the backbone, which is the same as approximating it by its long-term limit,  $h_0(T) = a^2$ . The calibration results for this six-parameter model are provided in Table 3. The fit degenerates noticeably by roughly 15 to 30 bps in RMSE, where the effect is stronger

**Figure 1: Calibrated implied volatility surfaces for tenors of 2, 5, 10, 20, and 30 years**



for shorter tenors, because the term structure of the backbone is more pronounced for those contracts. That was to be expected, because the forward swap rate can be rewritten in terms of a weighted sum of discrete forward rates (see, for example, Filipović, 2009, p. 14),

$$r_N(t, T) = \frac{\sum_{n=1}^N (T_n - T_{n-1}) P(t, T_n) F(t, T_{n-1}, T_n)}{A_{T,N}(t)}, \quad (39)$$

where  $F(t, T_{n-1}, T_n)$  is the forward rate for a deposit between  $T_{n-1}$  and  $T_n$  (possibly forward LIBOR), as seen from time  $t$ . The shorter the tenor, the less terms are contained in this sum, and the greater the influence of the term structure of the particular forward rates  $F(t, T_{n-1}, T_n)$ . Nevertheless, even the six-parameter model, which is effectively the stock market version, achieves a precision comparable to the original approach in Mazzoni (2015). The full model enhances the fit considerably.

## TECHNICAL PAPER

**Table 1: Implied volatility surface parameter estimates for different tenors**

Tenor	2y	5y	10y	20y	30y
RMSE	39.89 bps	41.77 bps	40.12 bps	41.65 bps	41.01 bps
$\omega$	$-5.16 \times 10^{-4}$	$-5.27 \times 10^{-4}$	$-6.61 \times 10^{-4}$	$4.04 \times 10^{-4}$	$2.13 \times 10^{-4}$
$\alpha$	0.5339	0.5557	0.5523	0.5078	0.4915
$\beta$	0.4708	0.4326	0.4508	0.5040	0.5130
$\gamma$	0.0626	0.0677	0.0645	0.0591	0.0590
$\Delta t$	1.6535	1.5609	1.5603	1.5349	1.5512
$a$	0.1138	0.1122	0.1041	0.0398	0.0762
$b$	0.1186	0.1027	0.0777	0.1126	0.0690
$c$	0.0117	0.0043	$4.59 \times 10^{-4}$	$9.27 \times 10^{-3}$	$9.47 \times 10^{-3}$
$d$	0.1824	0.1505	0.0811	0.0902	0.1287

**Table 2: Reduced model estimates with eight parameters**

Tenor	2y	5y	10y	20y	30y
RMSE	41.73 bps	44.30 bps	40.80 bps	41.58 bps	41.13 bps
$\omega$	$9.64 \times 10^{-3}$	$3.57 \times 10^{-4}$	$1.18 \times 10^{-3}$	$2.25 \times 10^{-3}$	$1.02 \times 10^{-3}$
$\alpha$	0.4727	0.5517	0.4943	0.4929	0.4936
$\beta$	0.5209	0.4209	0.5166	0.5325	0.5046
$\gamma$	0.1742	0.0438	0.1305	0.1079	0.0595
$\Delta t$	4.3572	0.8901	3.0147	2.8141	1.5548
$b$	0.2317	0.2102	0.1788	0.1530	0.1470
$c$	$-4.24 \times 10^{-6}$	$-4.93 \times 10^{-6}$	$-7.91 \times 10^{-6}$	$9.36 \times 10^{-3}$	$9.54 \times 10^{-3}$
$d$	0.0489	0.0414	0.0294	0.0714	0.0739

**Table 3: Reduced model estimates with six parameters**

Tenor	2y	5y	10y	20y	30y
RMSE	70.21 bps	66.79 bps	57.17 bps	55.33 bps	55.22 bps
$\omega$	$1.01 \times 10^{-5}$	$4.26 \times 10^{-6}$	$3.14 \times 10^{-5}$	$-6.72 \times 10^{-5}$	$-2.16 \times 10^{-4}$
$\alpha$	0.8492	0.8017	0.5936	0.5682	0.5376
$\beta$	0.1247	0.1764	0.3895	0.4208	0.4398
$\gamma$	$5.63 \times 10^{-3}$	$5.99 \times 10^{-3}$	0.0127	0.0144	0.0292
$\Delta t$	0.0972	0.0921	0.2278	0.3139	0.6582
$a$	0.2358	0.2089	0.1712	0.1520	0.1451

## 4 Performance of parametric volatility surface models

In this section, the suggested method is benchmarked against alternative parametric models for the entire volatility surface, as far as they are available in closed form.

### 4.1 The SVI parametrization of Gatheral and Wang

Gatheral and Wang (2012) introduced a parametrization of the local volatility surface that was motivated by stylized facts of those surfaces, generated by stochastic volatility models (SVI, “stochastic volatility inspired”). Indeed they added a term structure to the hyperbolic smile model introduced by Gatheral (2004). The

five-parameter formula for the local variance is

$$\sigma_{\text{loc}}^2(K, T) = a + b \left( \rho \left( \frac{\log(K/F_0)}{\sqrt{T}} - m \right) + \sqrt{\left( \frac{\log(K/F_0)}{\sqrt{T}} - m \right)^2 + \delta^2 T} \right). \quad (40)$$

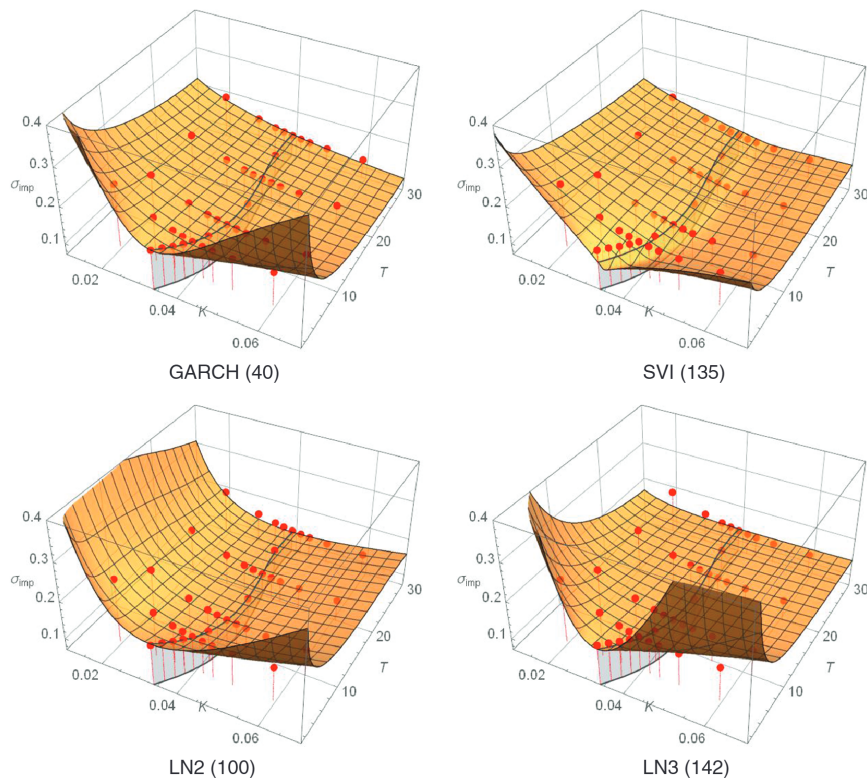
What is very appealing in this parametrization is that the respective quantities are directly related to particular properties of the volatility smile. That is:

- $a$  represents the overall level of variance,
- $b$  changes the angle between the left and right asymptotes,
- $\rho$  introduces skew,
- $m$  translates the backbone horizontally,

**Table 4: Calibration results for SVI parametrization**

Tenor	2y	5y	10y	20y	30y
RMSE	259.19 bps	198.69 bps	135.01 bps	108.32 bps	93.00 bps
$a$	0.0179	0.0160	0.0159	0.0145	0.0139
$b$	0.1704	0.1497	0.1224	0.1033	0.0943
$\rho$	0.0885	-0.0611	-0.2408	-0.4312	-0.4817
$m$	0.0384	0.0385	0.0311	0.0222	0.0215
$\delta$	$3.77 \times 10^{-7}$	$5.53 \times 10^{-5}$	$7.09 \times 10^{-5}$	$1.51 \times 10^{-6}$	$1.84 \times 10^{-7}$

**Figure 2: Different implied volatility surface models for 10-year tenor; approximate RMSE in parentheses (bps)**



- $\delta$  governs the smoothness of the vertex.

To obtain a closed-form expression for the implied variance, Eq. (40) is to be integrated along the most likely path. Under the premise that this path is sufficiently well approximated by a straight line in log-price space, one has to compute

$$\sigma_{\text{imp}}^2(K, T) = \frac{1}{T} \int_0^T \sigma_{\text{loc}}^2(F_0^{1-\frac{t}{T}} K^{\frac{t}{T}}, t) dt. \quad (41)$$

It is possible to evaluate the integral in Eq. (41). The resulting formula for the implied variance is provided in Appendix C. The calibration results for the SVI-implied volatility surface are given in Table 4. The RMSE is considerably larger than for all versions of the GARCH-parameterized volatility surface. In particular, the fit degenerates rapidly if the tenor of the underlying swap is short. That is because the term structure of the backbone becomes more pronounced and there is no mechanism in the SVI parametrization to accommodate this feature. A visual

## TECHNICAL PAPER

comparison of all approaches for the 10-year tenor slice of the volatility cube is provided in Figure 2.

### 4.2 The lognormal mixture model of Brigo and Mercurio

Brigo and Mercurio (2000, 2002) identified a class of analytically tractable mixture models, such that if the forward rate process is driftless under the measure  $Q$ , then the respective probability density satisfies

$$q(F, t) = \sum_{n=1}^N \lambda_n q_n(F, t). \quad (42)$$

They proved that for general diffusion terms  $v_n(F, t)$ , this leads under fairly mild conditions to a particular form of local variance,

$$\sigma_{\text{loc}}^2(F, t) = \sum_{n=1}^N \Lambda_n(F, t) \frac{v_n^2(F, t)}{F^2}, \text{ with } \Lambda_n(F, t) = \frac{\lambda_n q_n(F, t)}{\sum_{k=1}^N \lambda_k q_k(F, t)}. \quad (43)$$

For the canonical choice  $v_n(F, t) = \sigma_n(t)F$  and lognormal densities

$$q_n(F, t) = \frac{1}{F \sqrt{2\pi v_n^2(t)}} \exp\left(-\frac{1}{2}\left(\frac{\log(F/F_0) + \frac{1}{2}v_n^2(t)}{v_n(t)}\right)^2\right), \quad (44)$$

with

$$v_n(t) = \sqrt{\int_0^t \sigma_n^2(s) ds}, \quad (45)$$

the resulting call price is a weighted sum of Black-76 prices (cf. Brigo and Mercurio, 2007, p. 466), which makes the lognormal mixture particularly attractive.

To obtain an approximation for the implied volatility, Brigo and Mercurio (2007, p. 467) repeatedly apply Dini's implicit function theorem and Taylor-expand around  $K = F_0$ ,

$$\begin{aligned} \sigma_{\text{imp}}(K, T) &\approx \sigma_{\text{ATM}}(T) + \frac{\log^2(K/F_0)}{2\sigma_{\text{ATM}}(T)T} \\ &\times \sum_{n=1}^N \lambda_n \left( \frac{\sigma_{\text{ATM}}(T)\sqrt{T}}{v_n(T)} \exp\left(\frac{\sigma_{\text{ATM}}^2(T)T - v_n^2(T)}{8}\right) - 1 \right), \end{aligned} \quad (46)$$

where the ATM volatility is explicitly given by

$$\sigma_{\text{ATM}}(T) = \frac{2}{\sqrt{T}} \Phi^{-1} \left( \sum_{n=1}^N \lambda_n \Phi \left( \frac{v_n(T)}{2} \right) \right) \text{ and } \Phi(x) = \int_{-\infty}^x \frac{1}{\sqrt{2\pi}} e^{-z^2/2} dz. \quad (47)$$

Mixture models are generally not identifiable with respect to their particular components. Furthermore, their weights  $\lambda_n$  have to be non-negative and normalized. In the particular class of models introduced by Brigo and Mercurio (2000, 2002), there is an additional requirement: the volatility functions  $\sigma_n(t)$  have to be bounded from below and above by a strictly positive number for all  $t \geq 0$ . These requirements make the calibration process somewhat delicate. Therefore, two rather parsimonious mixture models were estimated: a two-densities mixture (LN2) with Nelson-Siegel volatility  $\sigma_n(t) = a_n + (b_n + c_n t)e^{-d_n t}$  and a three-densities mixture (LN3) with constant volatility  $\sigma_n(t) = a_n$ . The results are provided in Tables 5 and 6.

### 4.3 Comparison of alternative models

The LN2 has effectively nine free parameters, because the weights  $\lambda_n$  have to add up to one. It is therefore comparable to the full GARCH parametrization. The LN2, on the other hand, has five free parameters for the same reason, and is therefore very similar to the SVI parametrization. On average, SVI and LM3 perform similarly, although the SVI is far more vulnerable to a pronounced term structure of the backbone. The LN2 is mostly superior to the SVI, but none of the competing models perform nearly as well as even the reduced GARCH model with six parameters. The full model has an even smaller RMSE. To visualize the results, the full GARCH, SVI, LN2, and LN3 fit is illustrated in Figure 2 for the 10-year slice of the swaption cube. The approximate RMSE (in bps) is provided in parentheses. It is obvious that the GARCH parametrization provides an overall superior fit and reproduces the characteristic shapes of smile and skew.

### 5 Implied volatility and surface dynamics

Non-parametric implied volatility models experienced a severe setback due to a criticism of Hagan *et al.* (2002). They showed that these models induce wrong implied volatility dynamics and thus lead to improper hedges. In this section, their argument is summarized and subsequently it is shown that a parametric model, like the one introduced in this paper, overcomes this problem.

The argument of Hagan *et al.* (2002) is based on a perturbation series, linking local and implied volatility for a fixed time slice  $T$ ,

$$\sigma_{\text{imp}}(K, F_0) = \sigma_{\text{loc}} \left( \frac{F_0 + K}{2} \right) \left( 1 + \frac{1}{24} \frac{\sigma_{\text{loc}}'' \left( \frac{F_0 + K}{2} \right)}{\sigma_{\text{loc}} \left( \frac{F_0 + K}{2} \right)} (F_0 - K)^2 + \dots \right). \quad (48)$$

In Eq. (48) the time argument is omitted for notational brevity, and the dependence of implied volatility on the current forward price  $F_0$  of the underlying is made explicit. Derivatives with respect to the argument are indicated by primes. Because the second term on the right-hand side contributes only roughly 1 percent, the relation of local and implied volatility can largely be understood by focusing on the first term.

Assume that the model is calibrated today for a fixed expiry  $T$ , which mean that the observed smile is fitted by

$$\sigma_{\text{imp}}(K, F_0) = \sigma_{\text{obs}}(K), \quad (49)$$

where  $\sigma_{\text{obs}}(K)$  is some smooth function, interpolating the implied Black volatility for all observed strikes  $K$ . To recover local volatility, one has to use the calibrated implied smile and evaluate at  $K = 2F - F_0$ . Together with Eq. (48), one obtains

$$\sigma_{\text{loc}}(F) = \sigma_{\text{obs}}(2F - F_0)/(1 + \dots). \quad (50)$$

Now assume that the forward price changes,  $F_0 \rightarrow F_1$ . The local volatility model now induces the following implied volatility:

$$\sigma_{\text{loc}}(F) = \sigma_{\text{obs}}(2F - F_1)/(1 + \dots) = \sigma_{\text{obs}}(K - F_0 + F_1)/(1 + \dots), \quad (51)$$

and thus,

$$\sigma_{\text{imp}}(K, F_1) = \sigma_{\text{obs}}(K - F_0 + F_1). \quad (52)$$

From Eq. (52) it is very clear that if  $F_1 > F_0$ , which means the forward price of the underlying has moved to the right then the implied volatility smile is translated to

**Table 5: Calibration results for LN2 mixture model**

Tenor RMSE	2y 83.33 bps	5y 99.59 bps	10y 100.35 bps	20y 101.96 bps	30y 98.24 bps
$\lambda_1$	0.4242	0.4288	0.3135	0.2689	0.7012
$\lambda_2$	0.5758	0.5712	0.6865	0.7311	0.2988
$a_1$	0.0372	0.0755	0.0805	0.0793	0.1457
$d_2$	0.2441	0.2367	0.1605	0.1442	0.2737
$b_1$	0.1100	0.0757	0.0332	0.0189	$-4.24 \times 10^{-3}$
$b_2$	0.0655	0.0368	0.0604	0.0208	$-0.1448$
$c_1$	-0.0177	-0.0298	-0.0206	-0.0175	$-0.0265$
$c_2$	-0.0282	-0.0206	$1.36 \times 10^{-3}$	0.0403	0.0116
$d_1$	0.0980	0.1110	0.0833	0.0758	0.0869
$d_2$	0.1013	0.1010	0.2616	0.4817	0.9592

**Table 6: Calibration results for LN3 mixture model**

Tenor RMSE	2y 158.43 bps	5y 157.76 bps	10y 142.10 bps	20y 138.66 bps	30y 133.27 bps
$\lambda_1$	0.0456	0.0496	0.0382	0.0111	0.0116
$\lambda_2$	0.5356	0.9504	0.9376	0.0930	0.9848
$\lambda_3$	0.4188	0.0000	0.0242	0.8959	$3.60 \times 10^{-3}$
$a_1$	3.4127	1.5100	1.4204	3.6649	3.2302
$a_2$	0.1245	0.1180	0.1229	0.4228	0.1231
$d_3$	0.1245	0.0943	0.0329	0.0993	$2.46 \times 10^{-3}$

the left, and vice versa. This is the wrong direction and from the delta of the call option,

$$\Delta_C = \frac{\partial C_0^B}{\partial F_0} + \frac{\partial C_0^B}{\partial \sigma_{\text{imp}}} \frac{\partial \sigma_{\text{imp}}}{\partial F_0}, \quad (53)$$

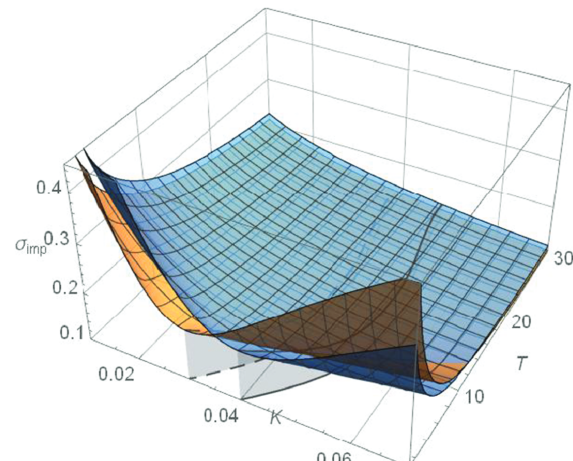
where  $C_0^B$  is the Black-76 price Eq. (1), it is immediately obvious that the second term on the right-hand side will have the wrong sign.

To see how this problem can be circumvented by a parametric model, one has to realize that in the non-parametric calibration step (49), the information about today's forward price is lost. The only argument of  $\sigma_{\text{obs}}(K)$  is the strike price. The GARCH parametrization suggested here is calibrated by estimating parameters, which govern distinct features of the implied volatility surface, relative to the forward price. As a result, the whole surface is shifted in the same direction as the forward price, as illustrated in Figure 3 for the 5-year tenor slice of the swaption example. The original forward swap rate (dashed backbone trace) was shifted by 1 percent in the positive direction (solid backbone trace). The respective implied volatility surfaces move along in the same direction. Thus, the GARCH parametrization overcomes the problem of generating wrong dynamics, inherent in non-parametrically fitted implied volatility surfaces, and therefore also provides correct hedges.

## 6 Summary and conclusions

In this paper, a highly flexible implied volatility surface parametrization was introduced. It is based on the theoretical observation that local variance is the conditional expectation of actual variance under the pricing measure, provided that the price process crosses the strike precisely at expiry. Computing this conditional

**Figure 3: Initial forward price  $F_0$  (yellow surface) is shifted to  $F_0 + 1\%$  (blue surface)**



## TECHNICAL PAPER

**Table A1: Discount bond data of September 28th, 2005**

T	P(0, T)	T	P(0, T)	T	P(0, T)
29-Sep-05	0.999942	30-Sep-10	0.870275	30-Sep-25	0.476246
03-Oct-05	0.999710	30-Sep-11	0.841442	30-Sep-26	0.456786
07-Oct-05	0.999470	28-Sep-12	0.812133	30-Sep-27	0.438279
31-Oct-05	0.998059	30-Sep-13	0.782237	29-Sep-28	0.420569
30-Nov-05	0.996281	30-Sep-14	0.752476	28-Sep-29	0.403782
21-Mar-06	0.989593	30-Sep-15	0.723171	30-Sep-30	0.387987
15-Jun-06	0.984243	30-Sep-16	0.694473	30-Sep-31	0.372828
21-Sep-06	0.977920	29-Sep-17	0.666446	30-Sep-32	0.358414
20-Dec-06	0.971923	28-Sep-18	0.639278	30-Sep-33	0.344706
20-Mar-07	0.965760	30-Sep-19	0.612743	29-Sep-34	0.331698
21-Jun-07	0.959287	30-Sep-20	0.587727	28-Sep-35	0.319318
20-Sep-07	0.952856	30-Sep-21	0.563523	29-Sep-45	0.217295
19-Dec-07	0.946414	30-Sep-22	0.540313	30-Sep-55	0.149179
30-Sep-08	0.925790	29-Sep-23	0.518115		
30-Sep-09	0.898422	30-Sep-24	0.496713		

expectation was possible by using a particular GARCH model with a modified bridge innovation. From this result, implied volatility was computed using the most likely path formalism of Gatheral (2006).

Because the suggested parametrization allows for a backbone of the Nelson–Siegel type, it is able to deal with the idiosyncrasies of underlyings in fixed-income markets. In particular, the typical hump-shaped or exponentially decaying form of ATM volatilities in those markets can easily be accommodated. This was demonstrated in an extended example, first introduced by Brigo and Mercurio (2007), encompassing the complete swaption cube data for expiries and tenors of up to 30 years and the corresponding fine-grained discount bond data. The suggested parametrization was calibrated to every tenor slice of the swaption cube and generated surfaces that reproduced the observed implied volatility with high accuracy. Subsequently, the quality of the fit was benchmarked against competing parametric models. None of them was able to reproduce the observed implied volatilities nearly as accurately as the suggested GARCH parametrization.

Finally, it was shown that the suggested model generates the correct dynamics if the forward price changes. As shown by Hagan *et al.* (2002), this is of vital importance, because otherwise the model is useless for hedging and risk management purposes. Furthermore, implied volatility can be computed analytically, without being influenced by any chosen interpolation scheme.

### Appendix A Proof of unconditional bridge expectation

To simplify the notation, the reference to the pricing measure and the bridge increment is suppressed in this appendix. The crucial step in proving Eq. (13) is to show that the relation

$$E[x_t] = \frac{n\Delta t}{T-t+n\Delta t} k + \frac{T-t}{T-t+n\Delta t} E[x_{t-n\Delta t}] \quad (\text{A.1})$$

holds for all  $n \leq \frac{t}{\Delta t}$ . For  $n = 0$ , Eq. (A.1) is trivially satisfied and for  $n = 1$ , one obtains

$$E[x_t] = E[E[x_t | \mathcal{F}_{t-\Delta t}]] = \frac{\Delta t}{T-t+\Delta t} k + \frac{T-t}{T-t+\Delta t} E[x_{t-\Delta t}]. \quad (\text{A.2})$$

To make the induction step, shift Eq. (A.2) from  $t$  to  $t - n\Delta t$  and plug the expectation back into Eq. (A.1) to obtain

$$\begin{aligned} E[x_t] &= \left( \frac{n\Delta t}{T-t+n\Delta t} + \frac{T-t}{T-t+n\Delta t} \cdot \frac{\Delta t}{T-t+(n+1)\Delta t} \right) k \\ &\quad + \frac{T-t}{T-t+n\Delta t} \cdot \frac{T-t+n\Delta t}{T-t+(n+1)\Delta t} E[x_{t-(n+1)\Delta t}] \\ &= \frac{n\Delta t(T-t+(n+1)\Delta t) + (T-t)\Delta t}{(T-t+n\Delta t)(T-t+(n+1)\Delta t)} k \\ &\quad + \frac{T-t}{T-t+(n+1)\Delta t} E[x_{t-(n+1)\Delta t}] \\ &= \frac{(n+1)\Delta t}{T-t+(n+1)\Delta t} k + \frac{T-t}{T-t+(n+1)\Delta t} E[x_{t-(n+1)\Delta t}]. \end{aligned} \quad (\text{A.3})$$

This proves the relation Eq. (A.1) and for  $n = \frac{t}{\Delta t}$ , one obtains Eq. (13).

### Appendix B Swaption cube example data

The data referenced in this section is bond and swaption data quoted in the EUR market on September 28th, 2005. Table A1 provides prices of zero bonds with unit principal (discount bonds), from which a continuous discount curve was extracted by cubic spline interpolation.

The respective forward swap rate was then computed by

$$r_N(t, T) = \frac{P(t, T_0) - P(t, T_N)}{\sum_{n=1}^N (T_n - T_{n-1}) P(t, T_n)}, \quad (\text{B.1})$$

where  $T = T_0$  is the expiry of the swaption. Because, in the euro area, interest rate swaps payments are semi-annual,  $N = 4$  means a 2-year tenor of the underlying swap contract for example.

**Table A2: ATM swaption volatility of September 28th, 2005**

Expiry	Tenor								
	1y	2y	3y	4y	5y	7y	10y	20y	30y
1y	21.50%	21.90%	21.50%	21.00%	20.40%	19.10%	17.60%	15.30%	14.60%
2y	21.60%	21.30%	20.70%	20.00%	19.50%	18.50%	17.30%	15.20%	14.70%
3y	20.90%	20.50%	19.80%	19.20%	18.60%	17.80%	16.80%	15.10%	14.60%
4y	20.00%	19.60%	18.90%	18.40%	17.80%	17.20%	16.40%	15.00%	14.40%
5y	19.10%	18.70%	18.10%	17.60%	17.20%	16.60%	16.00%	14.80%	14.30%
7y	17.80%	17.00%	16.60%	16.20%	15.90%	15.60%	15.20%	14.30%	14.00%
10y	15.90%	15.20%	14.80%	14.70%	14.60%	14.40%	14.40%	13.60%	13.10%
15y	14.10%	13.70%	13.50%	13.40%	13.30%	13.20%	13.20%	12.40%	12.00%
20y	13.20%	13.10%	13.10%	13.10%	13.10%	13.10%	13.10%	12.10%	11.90%
25y	12.90%	12.90%	13.00%	13.10%	13.10%	13.20%	13.10%	12.20%	12.20%
30y	13.00%	13.00%	13.00%	12.90%	12.90%	12.90%	12.90%	12.30%	12.30%

**Table A3: Swaption volatility smile of September 28th, 2005**

Expiry	Tenor	Strike								
		-200	-100	-50	-25	25	50	100	200	
5y	2y	8.71%	2.57%	0.93%	0.38%	-0.25%	-0.37%	-0.34%	0.29%	
10y	2y	5.73%	1.79%	0.64%	0.27%	-0.19%	-0.28%	-0.25%	0.27%	
20y	2y	5.32%	1.84%	0.74%	0.32%	-0.25%	-0.42%	-0.55%	-0.35%	
30y	2y	5.14%	1.76%	0.71%	0.32%	-0.26%	-0.44%	-0.64%	-0.60%	
5y	5y	8.64%	2.85%	1.10%	0.47%	-0.34%	-0.55%	-0.69%	-0.24%	
10y	5y	6.34%	2.22%	0.89%	0.39%	-0.31%	-0.51%	-0.69%	-0.45%	
20y	5y	5.62%	1.99%	0.81%	0.36%	-0.29%	-0.49%	-0.70%	-0.59%	
30y	5y	5.52%	1.93%	0.79%	0.35%	-0.29%	-0.49%	-0.72%	-0.70%	
5y	10y	7.80%	2.63%	1.02%	0.44%	-0.33%	-0.53%	-0.63%	-0.17%	
10y	10y	6.39%	2.25%	0.91%	0.40%	-0.31%	-0.52%	-0.71%	-0.47%	
20y	10y	5.86%	2.07%	0.85%	0.37%	-0.30%	-0.51%	-0.73%	-0.62%	
30y	10y	5.44%	1.92%	0.79%	0.35%	-0.29%	-0.52%	-0.79%	-0.85%	
5y	20y	7.43%	2.56%	1.00%	0.43%	-0.32%	-0.51%	-0.60%	-0.10%	
10y	20y	6.59%	2.34%	0.94%	0.41%	-0.32%	-0.54%	-0.72%	-0.43%	
20y	20y	6.11%	2.19%	0.90%	0.40%	-0.32%	-0.55%	-0.77%	-0.61%	
30y	20y	5.46%	1.92%	0.79%	0.35%	-0.29%	-0.50%	-0.72%	-0.69%	
5y	30y	7.45%	2.58%	1.01%	0.44%	-0.33%	-0.52%	-0.61%	-0.13%	
10y	30y	6.73%	2.38%	0.96%	0.42%	-0.33%	-0.53%	-0.68%	-0.35%	
20y	30y	6.20%	2.22%	0.91%	0.40%	-0.32%	-0.54%	-0.74%	-0.55%	
30y	30y	5.39%	1.90%	0.78%	0.35%	-0.28%	-0.50%	-0.72%	-0.68%	

Table A2 contains ATM swaption volatilities for different expiries and tenors, and Table A3 provides the associated smile data in terms of absolute difference in implied volatility with respect to the proper ATM volatility.

### Appendix C Explicit implied SVI surface formula

To compute the implied variance, it is convenient to introduce the new variable  $\alpha = \frac{t}{T}$ . With respect to this new variable Eq. (41) becomes

$$\sigma_{\text{imp}}^2(K, T) = \int_0^1 \sigma_{\text{loc}}^2(F_0^{1-\alpha} K^\alpha, \alpha T) d\alpha. \quad (\text{C.1})$$

This integral was computed and checked with Wolfram Mathematica and the result is

$$\begin{aligned} \sigma_{\text{imp}}^2(K, T) = & a - b m \rho + \frac{2b\rho \log(K/F_0)}{3\sqrt{T}} + \frac{b}{3A^5} \left[ 2AT^3\delta^2(Bm^2 - |m|^3 + bT\delta^2) \right. \\ & + AT\log^2(K/F_0)(|m|^3 - Bm^2 + 4BT\delta^2) - ABm\sqrt{T}\log^3(K/F_0) \\ & + 2AB\log^4(K/F_0) - \log(K/F_0) \left( ABmT^{5/2}\delta^2 + 3m^3T^3\delta^2 \right. \\ & \left. \left. \left. - m\log(K/F_0) \right) - \log \left( AB - m\log(K/F_0) + \frac{A^2}{\sqrt{T}} \right) \right] \right], \end{aligned} \quad (\text{C.2})$$

## TECHNICAL PAPER

with

$$A = \sqrt{T^2\delta^2 + \log^2(K/F_0)} \quad \text{and} \quad B = \sqrt{T^2\delta^2 + \left( \frac{\log(K/F_0)}{\sqrt{T}} - m \right)^2}. \quad (\text{C.3})$$

**Thomas Mazzoni** is a full professor of Economics and Finance at the University of Greifswald. He holds degrees in economics and business administration. After postgraduate studies in statistics and econometrics, he received a PhD for his work in the field of nonlinear filtering theory. In his scientific career, he has focused on problems from financial engineering and quantitative risk management.

### Endnote

1. However, some progress has been made recently. Gatarek *et al.* (2016) proposed a particular rolling maturity forward swap measure in the context of the two-factor Markovian HJM model of Cheyette (1992).

### References

- Bates, D. 1996. Jumps and stochastic volatility: The exchange rate processes implicit in Deutschemark options. *Review of Financial Studies*, 9, 69–107.
- Black, F. 1976. The pricing of commodity contracts. *Journal of Financial Economics*, 3, 167–179.
- Black, F. and M. Scholes 1973. The pricing of options and corporate liabilities. *Journal of Political Economy*, 81, 637–654.
- Bollerslev, T. 1986. Generalized autoregressive conditional heteroskedasticity. *Journal of Econometrics*, 31(3), 307–327.
- Brace, A., Gatarek, D., Musiela, M. 1997. The market model of interest rate dynamics. *Mathematical Finance*, 7(2), 127–147.
- Breeden, D. and Litzenberger, R. 1978. Prices of state-contingent claims implicit in option Prices. *Journal of Business*, 51, 621–651.
- Brigo, D. and Mercurio, F. 2000. A mixed-up smile. *Risk*, September: 123–126.
- Brigo, D. and Mercurio, F. 2002. Lognormal-mixture dynamics and calibration to market volatility Smiles. *International Journal of Theoretical & Applied Finance*, 5(4), 427–446.
- Brigo, D. and Mercurio, F. 2007. *Interest rate models – theory and practice*, 2nd edn. New York: Springer.
- Cheyette, O. 1992. Term structure dynamics and mortgage valuation. *Journal of Fixed Income*, 1(4), 28–41.
- Cox, J. C., Ingersoll, J. E. and Ross, S. A. 1985. A theory of the term structure of interest rate. *Econometrica* 53, 385–407.
- Derman, E. and Kani, I. 1998. Stochastic implied trees: Arbitrage pricing with stochastic term and strike Structure of Volatility. *International Journal of Theoretical and Applied Finance*, 1, 61–110.
- Dothan, L. U. 1978. On the term structure of interest rates. *Journal of Financial Economics*, 6(1), 59–69.
- Duan, J.-C. 1995. The GARCH option pricing model. *Mathematical Finance*, 5(1), 13–23.
- Dupire, B. 1994. Pricing with a smile. *Risk* 7, 18–20.
- Dupire, B. 1996. *A Unified Theory of Volatility*. Technical Report, Paribas Capital Markets.
- Dupire, B. 2004. A unified theory of volatility. *Derivatives Pricing: The Classic Collection*. London: Risk Books, pp. 185–196.
- Engle, R. F. 1982. Autoregressive conditional heteroskedasticity with estimates of the variance of United Kingdom inflation. *Econometrica* 50, 987–1008.
- Engle, R. F. 1990. Discussion: Stock market volatility and the crash of '87. *Review of Financial Studies* 3, 103–106.
- Filipović, D. 2009. *Term-structure models*. New York: Springer.
- Gatarek, D., Jablecki, J. and Qu, D. 2016. Non-parametric local volatility formula for interest rate swaptions. *Risk*, February: 120–124.
- Gatheral, J. 2004. A parsimonious arbitrage-free implied volatility parameterization with application to the valuation of volatility derivatives. Talk at the Global Derivatives & Risk Management Conference, Madrid, May 26, 2004.
- Gatheral, J. 2006. *The Volatility Surface – a Practitioner's Guide*. Hoboken, NJ: Wiley.
- Gatheral, J. and Wang, T.-H. 2012. The heat-kernel most-likely-path approximation. *International Journal of Theoretical and Applied Finance*, 15(1), 1250001–1–1250001–18.
- Hagan, P. S., Kumar, D., Lesniewski, A.S. and Woodward, D.E. 2002. Managing smile risk. *Wilmott Magazine* September, 84–108.
- Heath, D., Jarrow, R. and Morton, A. 1992. Bond pricing and the term structure of interest rates: A New Methodology for Contingent Claims Valuation. *Econometrica*, 60(1), 77–105.
- Heston, S. L. 1993. A closed-form solution for options with stochastic volatility with applications to bonds and currency options. *The Review of Financial Studies*, 6(2), 327–343.
- Heston, S. L. and Nandi, S. 1997. *A Closed-Form GARCH Option Pricing Model*. Technical Report, 97-9, Federal Reserve Bank of Atlanta.
- Heston, S. L. and Nandi, S. 2000. A closed-form GARCH option valuation model. *The Review of Financial Studies*, 13(3), 585–625.
- Jamshidian, F. 1997. LIBOR and swap market models and measures. *Finance and Stochastics* 1, 293–330.
- Keller-Ressel, M. and Teichmann, J. 2009. *A Remark on Gatheral's 'Most-Likely Path Approximation' of Implied Volatility*. Technical Report, TU Berlin.
- Mazzoni, T. 2015. A GARCH parametrization of the volatility surface. *Journal of Derivatives*, 23(1), 9–24.
- Merton, R. 1973. The theory of rational option pricing. *Bell Journal of Economics and Management Science* 4, 141–183.
- Merton, R. C. 1976. Option pricing when underlying stock returns are discontinuous. *Journal of Financial Economics* 3, 125–144.
- Nelson, C. R. and Siegel, A. F. 1987. Parsimonious modeling of yield curves. *Journal of Business*, 60(4), 473–489.
- Rebonato, R. 2004. *Volatility and Correlation*, 2nd edn. Chichester: Wiley.
- Rebonato, R., McKay, K. and White, R. 2009. *The SABR/LIBOR Market Model – Pricing, Calibration and Hedging for Complex Interest-Rate Derivatives*. Chichester: Wiley.
- Reghai, A. 2015. *Quantitative Finance – Back to Basic Principles*. Basingstoke Palgrave Macmillan.
- Vasicek, O. 1977. An equilibrium characterization of the term structure. *Journal of Financial Economics* 5, 177–188.

